

Negative capacitance effect in semiconductor devices

M. Ershov, *Member, IEEE*, H. C. Liu, L. Li, M. Buchanan, Z. R. Wasilewski, and A. K. Jonscher

Abstract— **Nontrivial capacitance behavior, including a negative capacitance (NC) effect, observed in a variety of semiconductor devices, is discussed emphasizing the physical mechanism and the theoretical interpretation of experimental data. The correct interpretation of NC can be based on the analysis of the time-domain transient current in response to a small voltage step or impulse, involving a self-consistent treatment of all relevant physical effects (carrier transport, injection, recharging etc.). NC appears in the case of the non-monotonic or positive-valued behavior of the time-derivative of the transient current in response to a small voltage step. The time-domain transient current approach is illustrated by simulation results and experimental studies of quantum well infrared photodetectors (QWIPs). The NC effect in QWIPs has been predicted theoretically and confirmed experimentally. The huge NC phenomenon in QWIPs is due to the non-equilibrium transient injection from the emitter caused by the properties of the injection barrier and the inertia of the QW recharging.**

I. INTRODUCTION

Capacitance characteristics provide a powerful spectroscopic method for the non-destructive testing of semiconductor devices and evaluation of their structural and physical parameters. Capacitance or admittance spectroscopy also give an insight into the device physics, provided that the experimental data are correctly interpreted. Quite often the capacitance exhibits highly non-trivial characteristics, most notable of which is the phenomenon of negative capacitance (NC). The NC effect has been displayed by a variety of electronic devices, both heterostructures and homostructures, made of crystalline or amorphous semiconductors, such as Si, Ge, GaAs, HgCdTe, Se, and others [1], [2], [3], [4], [5], [6], [7], [8], [9], [10], [11], [12], [13], [14], [15], [16], [17], [18], [19], [20], [21], [22], [23], [24], [25], [26], [27], [28], [29], [30], [31], [32], [33], [34], [35], [36], [37], [38]. These devices include p-n junctions, Schottky diodes, metal-insulator-metal devices, MESFETs, metal-insulator-semiconductor structures, weakly coupled superlattices, quantum mesoscopic devices, quantum well infrared photodetectors, and so on. Microscopic physical mechanisms of NC in different devices are, obviously, different, but there should be some general principle behind NC common to all types of devices. Although the physical origin of NC has been discussed in the literature [39], [40], the concept of NC is still not widely recognized. Moreover,

there is no adequate discussion of capacitance in classical texts on physics of semiconductor devices. The NC effect reported in the literature has been often referred to as “anomalous” or “abnormal”. NC measured experimentally has been sometimes (incorrectly) attributed to instrumental problems, such as parasitic inductance [41] or poor measurement equipment calibration [42]. Regrettably, in many cases experimental NC data were not reported in the literature due to the confusion caused by the NC effect. On the other hand, theoretical interpretations of the NC phenomenon were often based on considerations of purely electrostatic charge redistribution inside the device. However, a simple incremental charge method of capacitance calculation can be incorrect in the case of large conduction current (which often accompanies NC phenomenon), and more rigorous approaches considering transient response in the time or frequency domain should be used.

Recently, the NC effect in homogeneous (barrier-free) semiconductor structures has been considered theoretically in detail in ref. [43]. It was shown that NC can appear if the conductivity is inertial (i. e. current lags behind voltage) and the reactive component of the conduction current is larger than the displacement current. This situation can occur, for example, in structures with Drude conductivity, or in the case of impact ionization of impurity atoms. The real devices, however, contain contacts, which can influence strongly the small-signal characteristics and result in NC. Indeed, it was verified that in many cases the NC phenomenon was caused by the contact or interface effects (see, for example, ref. [22]).

In this work, we discuss the NC effect with an emphasis on the theoretical interpretation of this phenomenon. We obtain the general relationships between the transient current in the time-domain and capacitance in the frequency domain. These relationships, following from the properties of the Fourier transform, are independent of the particular physical processes and applicable to all types of electronic devices. The origin of NC is related to the non-monotonic or positive-valued behavior of the time-derivative of transient current upon application of a voltage step. We present the results of simulation and experimental studies of quantum well infrared photodetectors (QWIPs) displaying a huge NC. In QWIPs, this effect is due to the non-equilibrium transient injection from the emitter, caused by the properties of the injecting contact and inertia of the QW’s recharging processes.

M. Ershov is with the Department of Computer Software, University of Aizu, Aizu-Wakamatsu City 965-8580, Japan. E-mail: ershov@u-aizu.ac.jp .

H. C. Liu, L. Li, M. Buchanan, and Z. R. Wasilewski are with the Institute for Microstructural Sciences, National Research Council, Ottawa, Ontario K1A 0R6, Canada

A. K. Jonscher is with the Royal Holloway University of London, Egham, Surrey, TW20 0EX, UK

II. DEFINITION OF CAPACITANCE AND METHODS OF ITS CALCULATION

For simplicity, we consider two-terminal semiconductor devices. Capacitance is defined as

$$C(\omega) = \frac{1}{\omega} \text{Im}[Y(\omega)], \quad (1)$$

where

$$Y(\omega) = \frac{\delta I(\omega)}{\delta V(\omega)} \quad (2)$$

is the device admittance relating the small-signal harmonic current flowing through the terminals and small-signal voltage (δI , $\delta V \sim e^{i\omega t}$). The real part of the complex admittance is called conductance $G(\omega) = \text{Re}[Y(\omega)]$. In general, capacitance calculations should involve the solution of the system of equations describing device operation (Poisson equation, current continuity equation, etc.) in the time or frequency domain. There are several established methods for calculation of the capacitance (and, more generally, of the admittance) [44].

A. Incremental charge approach

In the incremental charge approach, steady-state equations describing device operation are solved for voltages V and $V + \Delta V$ (ΔV is small). The incremental charge distribution in the device $\delta Q(x)$ is separated into positive and negative components ΔQ and $-\Delta Q$, which are assigned to the respective contacts (the net charge increment inside the device is zero, according to the Gauss theorem). The capacitance is then calculated as $C = \Delta Q / \Delta V$. The main advantage of this method is its simplicity, as it requires only a steady-state simulation program for the calculation. However, there are several difficulties with this approach. One of the problems is that there is no rigorous procedure for the separation of incremental charge distribution into positive and negative parts, and its assignment to the contacts. This problem becomes especially important in the case of devices with more than two contacts and two- or three-dimensional geometry, as well as in the case when the incremental charge density of electrons and holes is distributed across the device area. Several heuristic approaches to tackle this problem have been proposed, without rigorous justification. Furthermore, this method allows the calculation only of the low-frequency value of the capacitance. More importantly, the incremental charge approach can be rigorously justified only if there is no conduction current in the device under DC conditions, which will be shown below. This approach can work well in the case of very low conduction current (as in reverse biased p-n junctions or Schottky diodes, MOS structures etc.). In the general case of non-zero DC current in the device, the incremental charge approach can fail, and its applicability in each particular case should be carefully examined.

B. Sinusoidal steady-state analysis

In the sinusoidal steady-state analysis (SSSA) approach, the system of the time-dependent equations is linearized

around a steady-state solution for harmonic small-signal quantities, and then solved for a particular frequency. The SSSA method is rigorous, rather simple to carry out, and fast. The disadvantage is that it requires solution of a system of equations for each frequency to obtain the frequency dependence of capacitance.

C. Method based on Fourier analysis

The method based on the Fourier analysis involves calculation of the transient response of the device to a small time-dependent voltage excitation (usually in the form of a step-function) applied at time $t = 0$. Admittance is calculated as the ratio of the Fourier components of the transient current $\delta I(t) = I(t) - I(0^-)$ and voltage $\delta V(t) = V(t) - V(0^-)$. The amplitude of the transient voltage should be chosen small enough to ensure the linearity of the transient effects. The particular value of the amplitude is dictated by the problem under consideration (it can be much less than the total applied voltage, thermal voltage, etc.) On the other hand, it should not be large enough that the transient current is properly resolved. This method is rigorous. It requires the solution of the transient problem only once to calculate the capacitance and conductance for any frequency. Its disadvantage is the stringent requirement on the choice of the time steps to obtain the proper frequency resolution and numerical accuracy [44]. The Fourier analysis method translates the small-signal problem from the frequency domain into the time domain. Although both the frequency-domain and time-domain representations are appropriate, the time-domain approach sometimes allows a more clear interpretation of the observed results in terms of the relevant physical effects. This method will be used in the next sections to relate the properties of the capacitance-frequency (C-F) characteristics to the time-domain behavior of the transient current, and to explain the origin of NC.

III. THE ORIGIN OF NEGATIVE CAPACITANCE

Let us consider transient current in a semiconductor device in response to an applied voltage step (see Fig. 1):

$$\delta V(t) \equiv V(t) - V(0^-) = \Delta V \theta(t), \quad (3)$$

$$\begin{aligned} \delta I(t) &\equiv I(t) - I(0^-) = \\ &[I(t) - I(\infty)] \theta(t) + [I(\infty) - I(0^-)] \theta(t), \end{aligned} \quad (4)$$

where $\theta(t)$ is the unity step function. The quantities with “+” and “-” superscripts denote single-sided values of the discontinuous functions, for example, $V(0^-) = \lim_{\tau \rightarrow 0} V(\tau)$, $\tau < 0$. In equation (4) we decomposed the transient current $\delta I(t)$ into the step-like component (DC conductivity) and transient current $\delta J(t) = [I(t) - I(\infty)] \theta(t)$, so that $\delta J(t) \rightarrow 0$ as $t \rightarrow \infty$. Substituting the Fourier expansions of eqs. (3) and (4) into formula (2), and noting that $\int_{-\infty}^{\infty} \theta(t) e^{-i\omega t} dt = 1/(i\omega)$ (strictly speaking, to ensure convergence of this integral, we must add to ω an

infinitesimal negative imaginary part, i. e. replace ω by $\omega - i0$), we obtain the following expression for admittance:

$$Y(\omega) = i\omega \int_0^\infty \delta I(t) e^{-i\omega t} dt. \quad (5)$$

Separating the real and imaginary parts in formula (5), we obtain the expressions for the capacitance and conductance:

$$C(\omega) = \frac{1}{\Delta V} \int_0^\infty \delta J(t) \cos \omega t dt. \quad (6)$$

$$G(\omega) = \frac{I(\infty) - I(0^-)}{\Delta V} + \frac{\omega}{\Delta V} \int_0^\infty \delta J(t) \sin \omega t dt. \quad (7)$$

In general, the transient current $\delta J(t)$ contains an impulse-like component and a slowly varying relaxation component (Fig. 1):

$$\delta J(t) = C_0 \Delta V \delta(t) + \delta j(t). \quad (8)$$

Here $\delta(t)$ is the delta-function. The impulse-like component corresponds to a current charging the geometric capacitance C_0 (which is also called a feedthrough capacitance or “cold” capacitance), assuming that application of a voltage step results in an instantaneous change of charges on the contacts. Physically, this current is due to the displacement current in the semiconductor. For a device with a 1D geometry, we have $C_0 = \varepsilon \varepsilon_0 A/L$, where ε is the (average) relative dielectric permittivity, ε_0 is the permittivity of vacuum, A is the area, and L is the distance between the contacts. The relaxation component $\delta j(t)$ can be due to the electron transport, trapping, impact ionization, and other physical processes. Substituting formula (8) into eqs. (6) and (7), we obtain the equations for capacitance and conductance in terms of the transient relaxation current $\delta j(t)$:

$$C(\omega) = C_0 + \frac{1}{\Delta V} \int_0^\infty \delta j(t) \cos \omega t dt. \quad (9)$$

$$G(\omega) = G(0) + \frac{\omega}{\Delta V} \int_0^\infty \delta j(t) \sin \omega t dt, \quad (10)$$

where $G(0) = (I(\infty) - I(0^-))/\Delta V$ is the DC or steady-state conductivity. It is useful to obtain an alternative formulation of eqs. (9) and (10). Using integration by parts, we get:

$$C(\omega) = C_0 + \frac{1}{\omega \Delta V} \int_0^\infty \left[-\frac{d\delta j(t)}{dt} \right] \sin \omega t dt. \quad (11)$$

$$G(\omega) = G(\infty) + \frac{1}{\Delta V} \int_0^\infty \left[\frac{d\delta j(t)}{dt} \right] \cos \omega t dt, \quad (12)$$

where $G(\infty) = [I(0^+) - I(0^-)]/\Delta V$ is the high-frequency conductivity. It can be shown that the derivative of the relaxation current $\delta h(t) = d\delta j(t)/dt$ corresponds to the relaxation component of transient current in response to

a voltage impulse (response function). Indeed, if $\delta H(t)$ is the transient current in response to a voltage impulse $\delta V(t) = v \delta(t)$ (v is the “power” of the voltage impulse), then the admittance is given by the formula $Y(\omega) = 1/v \int_0^\infty \delta H(t) e^{-i\omega t} dt$. Comparing this expression with formula (5), we obtain:

$$\delta H(t) = \frac{v}{\Delta V} \left\{ C_0 \Delta V \frac{d\delta(t)}{dt} + [I(0^+) - I(0^-)] \delta(t) + \frac{d\delta j(t)}{dt} \right\}. \quad (13)$$

The first term in eq. (13) corresponds to the displacement current, the second term corresponds to the instantaneous current response due to the high-frequency conductivity, and the last term is related to the relaxation current (see Fig. 2).

It is seen from eqs. (9)–(12) that the frequency dependence of capacitance and conductance is determined by the cosine and sine transforms of the transient current $\delta j(t)$ (and $\delta h(t)$), and, therefore, by the time-domain behavior of the transient current. If the function $\delta j(t)$ is positive-valued, and decreases monotonically and smoothly (without inflections) to zero as $t \rightarrow \infty$, then the integral in eq. (9) is positive, and the capacitance $C(\omega)$ is larger than C_0 at any frequency. Indeed, in this case the function $-d\delta j(t)/dt$ is positive and monotonically decreases to zero, so that the positive contribution to the integral in eq. (11) over the first half of a sine period outweighs the negative contribution over the second half of a period (see Fig. 3). On the other hand, if the function $-d\delta j(t)/dt$ is negative and monotonically increasing to zero, then the integral in eq. (11) is negative, capacitance $C(\omega)$ is less than C_0 , and can be negative. In the case of non-monotonic or positive-valued behavior of the derivative of the transient current, the capacitance can be negative in limited frequency ranges.

Thus, *the origin of NC is related to the non-monotonic or positive-valued behavior of the derivative of the transient current in response to a small voltage step*, as was first proposed by Jonscher [39].

IV. RELATIONS BETWEEN THE TRANSIENT CURRENT AND ADMITTANCE

Let us consider some other important relations between the frequency-dependent admittance and transient current following from the mathematical properties of the Fourier transform.

The low-frequency capacitance value is given by the following formula:

$$C(0) = C_0 + \frac{1}{\Delta V} \int_0^\infty \delta j(t) dt. \quad (14)$$

Thus, the value of the low-frequency incremental capacitance $\Delta C(0) = C(0) - C_0$ is determined by the net area under the curve $\delta j(t)$. If the net area is negative, the low-frequency capacitance $C(0)$ is less than C_0 and can be negative.

A sum rule complementary to eq. (14) reads:

$$\delta j(0^+) = \frac{2}{\pi} \int_0^\infty [C(\omega) - C_0] d\omega, \quad (15)$$

which follows immediately from the following relation for a function $f(t)$ such that $f(t) = 0$ if $t < 0$:

$$\int_0^\infty \text{Re}[f(\omega)] d\omega = \sqrt{\frac{\pi}{8}} f(0^+). \quad (16)$$

Therefore, the value of the relaxation current δj at $t = 0^+$ determines the total area under the curve of incremental capacitance $\Delta C(\omega) = C(\omega) - C_0$.

The high-frequency capacitance value is equal to the geometric capacitance:

$$C(\infty) = C_0, \quad (17)$$

because the integral of the product of a slowly varying function and fast oscillating harmonic function tends to zero as $\omega \rightarrow \infty$. From the physical viewpoint, this is due to the fact that at high frequencies the physical processes related to electron transport are “frozen” due to the finite inertia, and the total small-signal current at high frequencies contains only the displacement component associated with the charging of the geometric capacitance.

Let us further consider the asymptotic behavior of capacitance at high frequencies. Integrating eq. (9) by parts, we obtain:

$$C(\omega) = C_0 + \frac{1}{\Delta V} \delta j(t) \frac{\sin(\omega t)}{\omega} \Big|_0^\infty - \frac{1}{\omega \Delta V} \int_0^\infty t \frac{d\delta j(t)}{dt} \frac{\sin \omega t}{t} dt. \quad (18)$$

Since $\delta j(\infty) = 0$, the second term in (18) disappears. Further, by utilizing the following theorem for the function $f(t)$ satisfying Dirichlet's conditions ($f(t)$ has a finite number of maxima and minima in the interval, and has only a finite number of finite discontinuities):

$$\lim_{\omega \rightarrow \infty} \int_0^\infty f(t) \frac{\sin(\omega t)}{t} dt = \frac{\pi}{2} f(0^+), \quad (19)$$

we obtain the following relationship:

$$\lim_{\omega \rightarrow \infty} \{\omega [C(\omega) - C_0]\} = -\frac{1}{\Delta V} \frac{\pi}{2} \left(t \frac{d\delta j}{dt} \right)_{t=0^+}. \quad (20)$$

Therefore, the asymptotic behavior of the capacitance at $\omega \rightarrow \infty$ is determined by the sign of the time derivative of the relaxation current at $t = 0^+$. $C(\omega)$ approaches C_0 as $\omega \rightarrow \infty$ from above if $(d\delta j/dt)_{t=0^+} < 0$, and from below if $(d\delta j/dt)_{t=0^+} > 0$.

The relations between the frequency-dependent capacitance and transient current in response to a voltage step are very general and applicable to any type of electronic device, although the microscopic mechanism of the transient response can be quite different.

To illustrate these considerations, let us consider a simple yet very general type of transient response composed of negative and positive exponential components:

$$\Delta j(t) = \Delta V \{a_1 \exp(-t/\tau_1) - a_2 \exp(-t/\tau_2)\}, \quad (21)$$

where a_1 , a_2 , τ_1 and τ_2 are some parameters. The capacitance corresponding to this transient is calculated using eq. (9):

$$C(\omega) = C_0 + \frac{a_1 \tau_1}{1 + (\omega \tau_1)^2} - \frac{a_2 \tau_2}{1 + (\omega \tau_2)^2}. \quad (22)$$

Figure 4 shows the relaxation current and corresponding frequency-dependent capacitance for different values of the parameters listed in the inset of Fig. 4(a). It can be seen that, depending on values of the parameters, the frequency dependence of capacitance can be either monotonic with $C > 0$, or non-monotonic (if the transient current is non-monotonic) with $C < 0$ at low frequency, in accordance with the general theoretical considerations stated above.

It is interesting to note that relations similar to those considered in this section are true for the frequency-dependent conductance and transient current in response to an impulse-like voltage signal, which follows from the similarity of eqs.(9)–(10) and (11)–(12) (see also ref. [45]). Similar relationships can also be obtained by analyzing the transient voltage response to an excitation by a current impulse [46], [2].

V. NC IN QUANTUM WELL INFRARED PHOTODETECTORS

A. Device structure and physics

The physics of QWIPs has been extensively discussed in the literature [47], [48]. Fig. 5 shows the geometry and diagram of the physical processes in QWIP. The QWIP structure comprises the QW region including doped QWs separated by undoped barriers. The QW structure is clad with the emitter and collector contacts. Under applied voltage, electrons are injected from the emitter and drift towards the collector. Electrons can be captured by the QWs and emitted from the QWs to the continuum due to thermoexcitation (we consider dark current conditions here). The value of the electric field at the injecting contact is controlled by the recharging of the QWs near the emitter to equilibrate the injection current and drift current in the bulk of QWIP. Our preliminary simulations of QWIPs showed that the capacitance can be negative for some voltage and frequency ranges. This result was surprising, since the NC phenomenon has never been reported in QWIPs before, even though these devices have been actively studied over the last decade. Therefore, we checked this result experimentally to exclude the possibility of simulation artifacts.

B. Experimental data

The results presented here were obtained on a GaAs/Al_{0.251}Ga_{0.749}As QWIP with 4 QWs of 62 Å width, separated by barriers of 241 Å width. The barriers were undoped, and the QWs were center δ -doped with silicon

to about $9 \times 10^{11} \text{ cm}^{-2}$. The GaAs contacts doped to $1.5 \times 10^{18} \text{ cm}^{-3}$ were separated from the QW structure by rectangular barriers identical to inter-well barriers. The geometric capacitance was $C_0 = 10.9 \text{ pF}$ for a mesa device of $120 \times 120 \text{ }\mu\text{m}^2$ in size. All measurements were performed at a temperature of $T=80 \text{ K}$. Devices were mounted on a test package with equivalent open and short wires for reference. HP4284A (20 Hz–1 MHz) and 4285A (75 kHz–30 MHz) Precision LCR meters were used for the C-V and C-F measurements. We checked carefully that parasitic elements did not influence the measurement data. Static characteristics of this QWIP were reported in ref. [49].

Figure 6 shows C-V characteristics measured at different frequencies. For the lowest frequency of 0.1 kHz the capacitance displays a maximum at zero bias. With an increase of voltage the capacitance decreases rapidly, approaching negative values. The capacitance does not decrease monotonically with voltage but displays peaks and shoulders. The capacitance at zero bias decreases with frequency, approaching the value of the geometric capacitance at frequencies $f \geq 10^2\text{--}10^3 \text{ kHz}$. C-V characteristics at intermediate frequencies ($1 \text{ kHz} \leq f \leq 100 \text{ kHz}$) are similar to low-frequency characteristics. The decrease of capacitance with voltage becomes less steep, and the voltage at which $C=0$ increases with frequency. At the highest measurement frequencies $f \geq 1 \text{ MHz}$ the capacitance is constant and equal to C_0 at low voltage, and exhibits an overshoot at high voltages, with a subsequent steep decrease. For this frequency range, the capacitance does not reach negative values at negative bias, as it would require too high a voltage, causing device heating.

The frequency dependence of the capacitance is shown in Fig. 7 using two different vertical scales. The magnitudes of the NC values are plotted in the log plot (Fig. 7(b)). At very low frequencies ($f \leq 100 \text{ Hz}$) the capacitance data are very noisy and not plotted. The capacitance at low bias voltages ($|V| \leq 0.1 \text{ V}$) is positive and decreases with frequency to the value of C_0 . For a higher voltage ($V = -0.2 \text{ V}$), the capacitance starts with negative values at low frequencies and increases monotonically above zero, approaching the C_0 value at high frequencies. With the further increase of voltage ($V = -0.49 \text{ V}$) the capacitance dependence on frequency becomes non-monotonic and develops a broad maximum. The magnitude and frequency location of its maximum depend on the applied voltage. The absolute value of the negative capacitance at low frequencies increases rapidly with voltage, and can exceed the geometric capacitance by more than two orders of magnitude (Fig. 7b).

Measurements on QWIPs having 8, 16 and 32 QWs gave a similar capacitance behavior as a function on bias voltage and frequency, but the peaks on the C-V curves were less pronounced.

C. Simulation results

We performed the simulation with the use of a time-dependent QWIP simulator based on the numerical model described in ref. [50]. The capacitance was calculated using

the Fourier transform of the transient current (see eq. (9)) obtained from the solution of the time-dependent problem on application of a small voltage step ($\Delta V=5 \times 10^{-3} \text{ V}$) to the QWIP. Calculated C-V and C-F characteristics are shown in Fig. 8. We would like to point out the very good qualitative agreement of the simulation results and experimental data by comparing Fig. 8 with Figs. 6 and 7. However, there are some quantitative discrepancies, including the magnitude of the low-frequency capacitance at low voltage, the width and magnitude of the capacitance peaks in the C-V and C-F characteristics, the magnitude of the negative capacitance, and the frequencies at which $C=0$. In our computational experiments we found that these features are *very* sensitive to the parameters of the simulation model (such as the QW capture velocity, field-dependent mobility, escape time from the QWs, etc.) and on the operating temperature. However, the main features of the capacitance behavior are independent of the variation of model parameters and temperature: at low voltages capacitance at low frequency is positive and decreases to the geometric capacitance at high frequency; capacitance at high voltages is negative at low frequency and increases with frequency to reach the geometric capacitance; the magnitude of the negative capacitance strongly increases with voltage and can exceed the geometric capacitance by a few orders of magnitude; and the voltage at which $C=0$ increases with increasing frequency. Since the model parameters are not available, and taking into account a significant asymmetry of experimental C-V characteristics, we focused not on the fitting of simulation results to experimental data, but on the explanation of the unusual features of the QWIP capacitance and the underlying physics.

As we discussed above, the clue to the capacitance behavior in the frequency domain is in the time-domain transient current. Figure 9 shows the calculated transient current for several applied voltages. The relaxation component of the transient current is positive and monotonic at low voltages, which results in positive capacitance at any frequency in the low voltage range (Fig. 8(a)). At high voltages, the transient current is dominated by a negative component, whose amplitude increases with voltage (Fig. 8(b)). Since the low-frequency capacitance is directly related to the transient current, this results in negative low-frequency capacitance, which increases strongly in magnitude with bias. The high-frequency capacitance tends to the geometric capacitance. Physically, this is due to the fact that the QW recharging processes determining the capacitance are “frozen” at frequencies higher than the inverse characteristic time of QW recharging.

We now give a physical picture of the transient current behavior. The transient current after the application of a voltage step is due to several effects resulting from an instantaneous increase of the electric field, such as enhanced electron emission from the QWs, increased drift electron velocity, and non-equilibrium electron injection from the emitter. The combined influence of these effects on transient current can be quite complicated in general, and their relative importance depends strongly on

applied voltage. At high applied voltages ($|V| \geq 0.2$ V for the present 4-well sample) the effect of the non-equilibrium transient injection is the dominant one in determining the behavior of the transient current, including negative current $\delta j(t) < 0$. To illustrate this effect, we plot in Fig. 10 the dependence of the electric field in the emitter barrier E_e on the average electric field $E_a(V) = V/L$ along with its derivative $dE_e/dE_a(V)$ under steady-state conditions. It is seen that $dE_e/dE_a > 1$ at any E_a for the QWIP under consideration. This effect results from the difference of the current-electric field characteristics in the injecting contact and the bulk QW region. [48] Note that just after the application of a voltage step ΔV to the QWIP, the instantaneous change of the electric field is constant over the QWIP structure and equal to $\Delta E = \Delta V/L$. This means that at the beginning of the transient, the electric field in the emitter barrier $E_e(V) + \Delta E$ is *lower* than the steady-state electric field $E_e(V + \Delta V)$ corresponding to the new voltage $V + \Delta V$ (see Fig. 11). Therefore, the injection (conduction) current is *lower* than the steady-state current, resulting in a negative transient current δj . The transient current at high voltage is dominated by the conduction component. The magnitude of the negative transient current at time $t = 0^+$ is equal approximately to $d j_{inj}/dE_e \times [E_e(V + \Delta V) - (E_e(V) + \Delta E)]$, and increases strongly with voltage due to an exponential dependence of injection current $j_{inj}(E_e)$ [48]. During the transient, the QWs are recharged and the current tends to its steady-state value. Thus, the non-monotonic and negative-valued behavior of δj , responsible for the negative capacitance, are due to the non-equilibrium transient injection from the emitter upon application of a voltage step.

At low voltage, the conductance of the QWIP is low, and the transient current is dominated by the displacement component related to the release and escape of electrons from the QWs.

It should be noted that transient current characteristics are determined by the $E_e(E_a)$ behavior, and therefore, by the injecting property of the emitter. Depending on the structural parameters of the injecting barrier, the derivative $dE_e/dE_a(V)$ can be either greater or less than unity, thus making the transient current negative or positive. Our simulations show that QWIPs with a triangular emitter barrier [51] have $dE_e/dE_a < 1$. The transient current in these QWIPs is positive, and their capacitance is always positive at all frequencies and voltages. In this respect, QWIPs with triangular emitter and multiple QWs are similar to the single QW phototransistor considered earlier [52], [53].

Thus, the negative-valued behavior of the transient current in the QWIP in response to a voltage step and the NC is due to the non-equilibrium transient injection from the emitter.

We have to point out that some features of the experimental data on QWIP capacitance are still unexplained. Simulation predicts the saturation of NC at low frequencies (Fig. 8(b)), while experimental data shows a strong increase of the absolute value of NC proportional to $1/\omega$ at

low frequencies (Fig. 7(b)). A similar behavior of NC has also been reported in other semiconductor devices [22], [40], but the physical mechanism of this low-frequency behavior of QWIP capacitance is not clear. This phenomenon confirms a close relation between the NC effect and the effect of the low-frequency dispersion observed in a great variety of semiconductor devices and other physical systems [40].

VI. DISCUSSION

A negative capacitance C has the same phase relationship between the small-signal voltage and current as a positive inductance $L = -1/\omega^2 C$. However, the interpretation of negative capacitance in terms of conventional inductance is not physically meaningful for the following reasons. First, in the case of “normal” inductance the behavior is associated with the magnetic field, which is not relevant for our consideration. Second, the impedance of “normal” inductance $|Z| = \omega L$ increases with frequency and, therefore, should dominate at high frequencies. However, the semiconductor devices under consideration display normal capacitance behavior ($C = C_0 > 0$) at high frequency. In this regard, the interpretation of the NC effect in terms of parasitic series inductances [41] or poor measurement equipment calibration [42] is incorrect. If, to the contrary, high-frequency capacitance is negative, and the imaginary part of the impedance is proportional to the frequency $|Z| \sim \omega$, this is a clear indication of the dominant role of parasitic inductance of the external circuit (see, for example, ref. [54]). Thus, measurement of the device admittance (or impedance) in a wide frequency range, and its behavior at high frequencies tests whether the NC effect is due to internal properties of the device or due to the parasitic inductance.

A term “negative capacitance” is often used to emphasize the inductive behavior of a device, which is expected to display (or usually displays) capacitive response. Complementary, a term “negative inductance” is used to emphasize capacitive behavior of some devices (see, for example, ref. [55]).

A note should be made concerning the physical interpretation of capacitance and the methods of its calculation in semiconductor devices. Conventionally, capacitance is associated with the accumulation of charges and electric field energy with the change of the voltage on contacts. This concept comes from electrostatics, when the conduction current is zero and the total electric current is due to the displacement component, related to the redistribution of charges inside the structure. However, the capacitance is determined by the reactive part of the *total* current, which comprises both conduction and displacement components. To distinguish the notion of “true” capacitance and “electrostatic” capacitance, a new term “emittance” has been introduced recently [34]. These two concepts are equivalent only if the conduction component of the reactive current is much lower than the displacement component. Indeed, let us suppose that the conduction component of the transient current $\Delta I(t)$ is zero at some cross-section (in the 1D geometry), i. e. the transient current contains only the dis-

placement component $\Delta I(t) = A\varepsilon\varepsilon_0\partial E/\partial t$. Substituting this expression into formula (6), we obtain (for the case $\omega = 0$) $C(0) = A\varepsilon\varepsilon_0\Delta E/\Delta V = \Delta Q/\Delta V$, where ΔQ is the charge increment at the each side of that cross-section. Therefore, the incremental charge approach to the capacitance calculation (for the case $\omega = 0$) is correct, if there is a cross-section inside the device where the conduction current is zero (in devices with multi-dimensional geometry (2D or 3D) and many contacts, low-frequency capacitance of a contact can be rigorously calculated using this approach if the contact is non-conducting in DC regime).

If the contribution of the conduction current to the reactive current is larger than that of the displacement current (this is usually the case for devices displaying NC), the capacitance is determined by the current which passes through the structure without charging effects, and capacitance has no relation to charge or energy accumulation. In this case, approaches of capacitance calculation based on static device characteristics (such as the incremental charge partitioning approach [44]) are incorrect, and the rigorous methods such as Fourier decomposition of transient excitation or SSSA [44] should be used.

It is worthwhile to mention a confusion caused by two different conventions for defining the complex phase factor for small-signal harmonic quantities (current, voltage, etc.). In this paper we followed the electrical (+) convention $\delta I, \delta V \sim \exp(i\omega t)$. In this convention, *capacitive* response (positive capacitance) corresponds to *positive* reactive part of admittance (susceptance). The physics (−) convention uses the phase factor $\exp(-i\omega t)$, which corresponds to *capacitive* response if susceptance is *negative* (capacitance is defined as $C = -\frac{1}{\omega}\text{Im}[Y(\omega)]$ in physics convention). Note that admittances (eq. (2)) corresponding to (+) and (−) conventions are complex conjugate quantities: $Y_+(\omega) = Y_-(\omega)$. However, important physical quantities (which can be measured or calculated) and relationships (such as phase relationship between current and voltage) are independent of the choice of the sign convention.

VII. CONCLUSIONS

The effect of NC in semiconductor devices is discussed. The relations between the transient relaxation current in the time-domain in response to a voltage step or impulse and capacitance in the frequency-domain are outlined. NC appears if the time-derivative of the transient current in response to a voltage step is positive-valued or non-monotonic with time. The incremental charge method of capacitance calculation is *absolutely inapplicable* in the case of large conduction current in the device, which is often the case when the capacitance is negative. The correct interpretation of NC should be based on rigorous approaches such as SSSA or Fourier analysis of the transient current. These points are illustrated by the results of experimental and theoretical studies of small-signal characteristics of QWIPs, which exhibit a huge NC. NC and peaks on the C-V and C-F curves are explained in terms of the transient current, which has a positive-valued time-derivative of transient current in the time-domain. This behavior is

due to the non-equilibrium transient electron injection from the emitter, which is determined by the inertia of the QWs' recharging processes and injection properties of the emitter barrier.

ACKNOWLEDGMENTS

This work has been partially supported by Electronic Communication Frontier Research and Development Grant of Ministry of Post and Telecommunications, Japan, by the Research Fund of the University of Aizu, and by Defence Research Establishment Valcartier, Department of National Defence, Canada. We thank P. Chow-Chong and P. Marshall of NRC for sample fabrication. One of the authors (M. E.) thanks M. Büttiker, M. J. Morant, and M. Stockman for useful discussions.

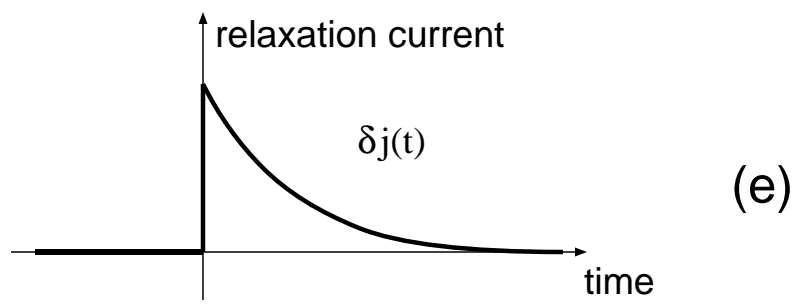
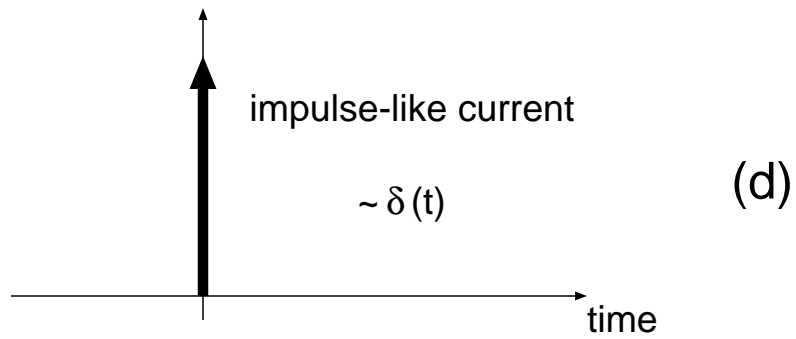
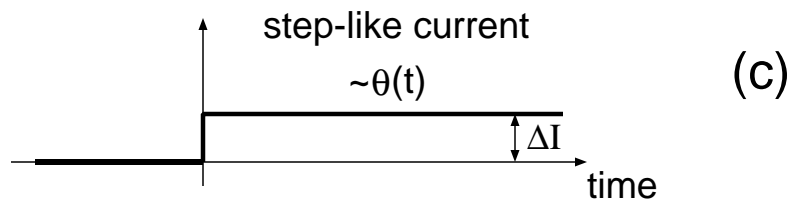
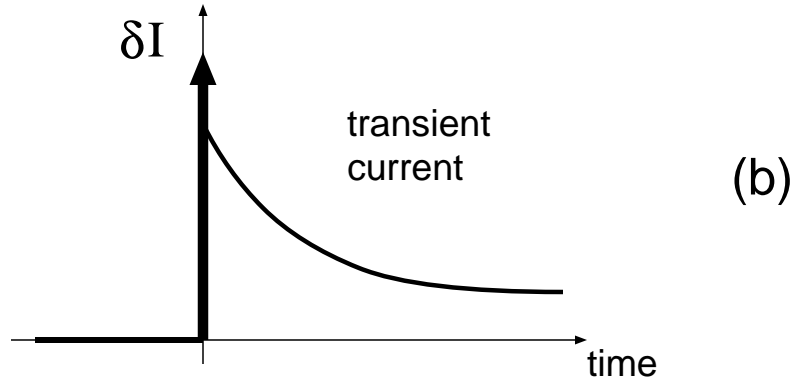
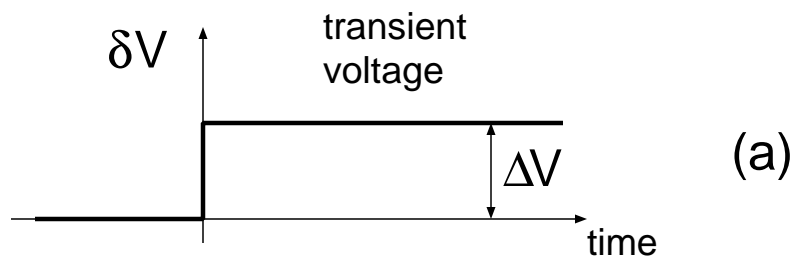
REFERENCES

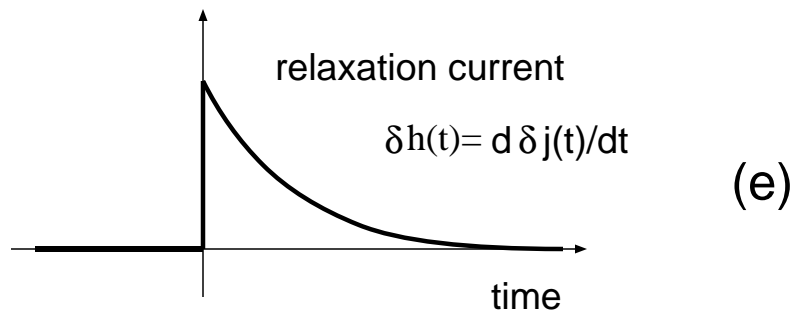
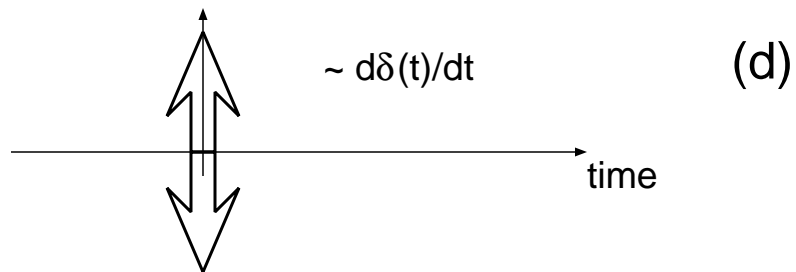
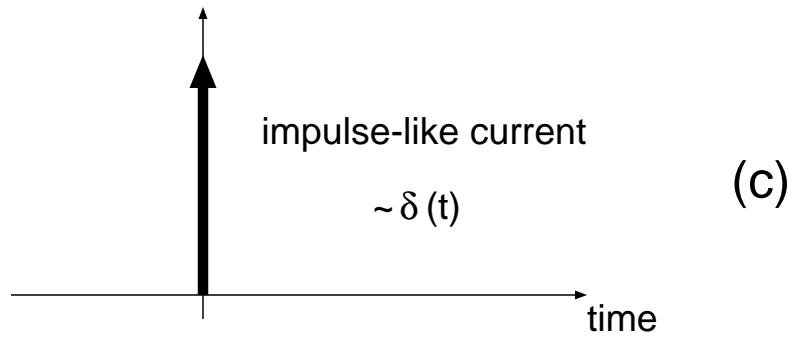
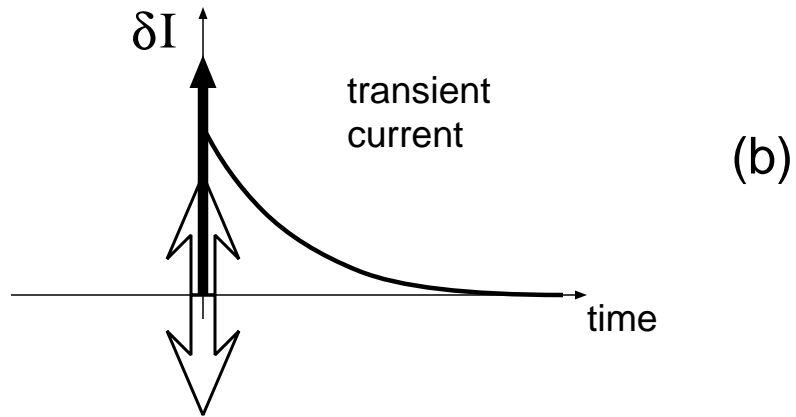
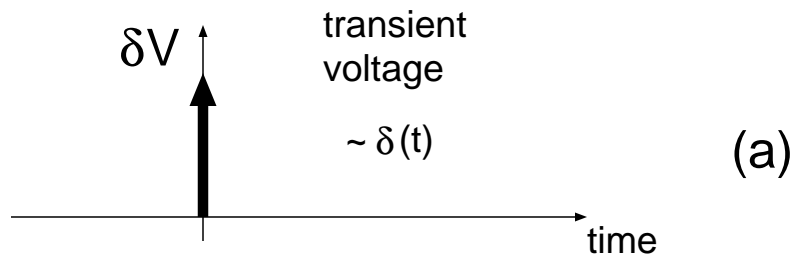
- [1] Y. Kanai, "On the inductive part of the a. c. characteristics of the semiconductor diodes," *J. Phys. Soc. Japan*, vol. 10, pp. 718–720, 1955.
- [2] T. Misawa, "Impedance of bulk semiconductor in junction diode," *J. Phys. Soc. Japan*, vol. 12, pp. 882–890, 1957.
- [3] T. Misawa, "Negative resistance in p-n junctions under avalanche breakdown conditions, Part I," *IEEE Trans. Electron Devices*, vol. 13, no. 1, pp. 137–141, 1966.
- [4] T. Misawa, "Negative resistance in p-n junctions under avalanche breakdown conditions, Part II," *IEEE Trans. Electron Devices*, vol. 13, no. 1, pp. 141–153, 1966.
- [5] R. F. Kazarinov, V. I. Stafeev, and R. A. Suris, "Impedance and transient processes in germanium diodes with deep levels," *Sov. Phys. Semicond.*, vol. 1, no. 9, pp. 1084–1086, 1967.
- [6] O. J. Marsh and C. R. Viswanathan, "Space-charge-limited current of holes in silicon and techniques for distinguishing double and single injection," *J. Appl. Phys.*, vol. 38, no. 8, pp. 3135–3144, 1967.
- [7] R. Vogel and P. J. Walsh, "Negative capacitance in amorphous semiconductor chalcogenide thin films," *Appl. Phys. Lett.*, vol. 14, no. 7, pp. 216–218, 1969.
- [8] H. K. Rockstad, "Ionization model for negative capacitance in low-mobility semiconductors such as amorphous chalcogenides," *J. Appl. Phys.*, vol. 42, no. 3, pp. 1159–1166, 1971.
- [9] J. Allison and V. R. Dave, "Frequency dependence of negative-capacitance effects observed in amorphous semiconductor thin-film devices," *Electron. Lett.*, vol. 7, no. 24, pp. 706–707, 1971.
- [10] S. A. Altunyan, V. S. Minaev, V. I. Stafeev, L. S. Gasanov, A. S. Deshevoi, and B. K. Skachkov, "An investigation of the electrical characteristics of memory and nonmemory switching devices made of chalcogenide glasses," *Sov. Phys. Semicond.*, vol. 5, no. 3, pp. 427–430, 1971.
- [11] V. A. Brodovoi and N. Z. Derikot, "Investigation of the impedance of GaAs:Cu in strong electric fields," *Sov. Phys. Semicond.*, vol. 7, no. 4, pp. 459–461, 1973.
- [12] B. T. Kolomiets, A. Ya. Karachentsev, and V. V. Spevak, "Investigation of surface barriers in silicon carbide single crystals," *Sov. Phys. Semicond.*, vol. 7, no. 7, pp. 872–875, 1974.
- [13] G. A. Egiazaryan and V. I. Stafeev, "Some properties of S-type diodes made of semiinsulating gallium arsenide," *Sov. Phys. Semicond.*, vol. 9, no. 3, pp. 334–336, 1975.
- [14] A. S. Deshevoi and L. S. Gasanov, "Solid-state inductance of amorphous and compensated semiconductors," *Sov. Phys. Semicond.*, vol. 11, no. 10, pp. 1168–1170, 1977.
- [15] A. I. Veinger, "Contact with a negative differential capacitance in the form of hot-carrier p-n junction," *Sov. Phys. Semicond.*, vol. 12, no. 10, pp. 1180–1182, 1978.
- [16] T. Noguchi, M. Kitagawa, and I. Taniguchi, "Negative capacitance of silicon diode with deep level traps," *Jpn. J. Appl. Phys.*, vol. 19, no. 7, pp. 1423–1424, 1980.
- [17] G. S. Nadkarni, N. Sankarraman, and S. Radhakrishnan, "Switching and negative capacitance in Al-Ge₁₅Te₈₁Sb₂S₂-Al devices," *J. Phys. D*, vol. 16, pp. 897–908, 1983.
- [18] V. N. Alimpiev and I. R. Gural'nik, "Negative capacitance of a photosensitive semiconductor," *Sov. Phys. Semicond.*, vol. 18, no. 4, pp. 420–422, 1984.
- [19] G. Blatter and F. Greuter, "Electrical breakdown at semiconductor grain boundaries," *Phys. Rev. B*, vol. 34, no. 12, pp. 8555–8572, 1986.
- [20] A. K. Jonscher, C. Pickup, and S. Zaidi, "Dielectric spectroscopy of semi-insulating gallium arsenide," *Semicond. Sci. Technol.*, vol. 1, pp. 71–92, 1986.
- [21] S.-T. Fu and M. B. Das, "Backgate-induced characteristics of ion-implanted GaAs MESFET's," *IEEE Trans. Electron Devices*, vol. 34, no. 6, pp. 1245–1252, 1987.
- [22] A. K. Jonscher and M. N. Robinson, "Dielectric spectroscopy of silicon barrier devices," *Solid-State Electron.*, vol. 31, no. 8, pp. 1277–1288, 1988.
- [23] J. Werner, A. F. J. Levi, R. T. Tung, M. Anzlowar, and M. Pinto, "Origin of the excess capacitance at intimate Schottky contacts," *Phys. Rev. Lett.*, vol. 60, no. 1, pp. 53–56, 1988.
- [24] X. Wu and E. S. Yang, "Interface capacitance in metal-semiconductor junctions," *J. Appl. Phys.*, vol. 65, no. 9, pp. 3560–3567, 1989.
- [25] L. He and T. Dingyuan, "Capacitance-voltage characteristics of p-n junction of the narrow band-gap semiconductors Hg_{1-x}Cd_xTe," *Chinese Physics*, vol. 9, no. 1, pp. 223–230, 1989.
- [26] X. Wu, H. L. Ebans, and E. S. Yang, "Negative capacitance at metal-semiconductor interfaces," *J. Appl. Phys.*, vol. 68, no. 6, pp. 2845–2848, 1990.
- [27] C. H. Champness and W. R. Clark, "Anomalous inductive effect in selenium Schottky diodes," *Appl. Phys. Lett.*, vol. 56, no. 12, pp. 1104–1106, 1990.
- [28] R. Merlin and D. A. Kessler, "Photoexcited quantum wells: Nonlinear screening, bistability, and negative differential capacitance," *Phys. Rev. B*, vol. 41, no. 14, pp. 9953–9957, 1990.
- [29] P. Muret, D. Elguennouni, M. Missous, and E. H. Rhoderick, "Admittance of Al/GaAs Schottky contacts under forward bias as a function of interface preparation conditions," *Appl. Phys. Lett.*, vol. 58, no. 2, pp. 155–157, 1991.
- [30] M. J. Morant and B. Y. Majlis, "A silicon negative resistance, negative capacitance device," in *Proc. of the IEEE Int. Conf. on Semiconductor Electronics*, 1992.
- [31] M. Beale and P. Mackay, "The origins and characteristics of negative capacitance in metal-insulator-metal devices," *Philosophical Magazine B*, vol. 65, no. 1, pp. 47–64, 1992.
- [32] M. Beale, "Anomalous reactance behaviour during the impedance analysis of time-varying dielectric systems," *Philosophical Magazine B*, vol. 65, no. 1, pp. 65–77, 1992.
- [33] A. P. Boltaev, T. M. Burbaev, G. A. Kalyuzhnaya, V. A. Kurbatov, and N. A. Penin, "Negative capacitance in Ni-TiO₂-p-Si heterostructures," *Russian Microelectronics*, vol. 24, no. 4, pp. 255–258, 1995.
- [34] T. Christen and M. Büttiker, "Low frequency admittance of a quantum point contact," *Phys. Rev. Lett.*, vol. 77, no. 1, pp. 143–146, 1996.
- [35] S. Ezhilvalavan and T. R. N. Kutty, "High-frequency capacitance resonance of ZnO-based varistor ceramics," *Appl. Phys. Lett.*, vol. 69, no. 23, pp. 3540–3542, 1996.
- [36] M. Ershov, H. C. Liu, L. Li, M. Buchanan, Z. R. Wasilewski, and V. Ryzhii, "Unusual capacitance behavior of quantum well infrared photodetectors," *Appl. Phys. Lett.*, vol. 70, no. 14, pp. 1828–1830, 1997.
- [37] K. Misiakos, D. Tsamakis, and E. Tsoi, "Measurement and modeling of the anomalous dynamic response of high resistivity diodes at cryogenic temperatures," *Solid-State Electron.*, vol. 41, no. 8, pp. 1099–1103, 1997.
- [38] I. Omura, H. Ohashi, and W. Fichtner, "IGBT negative gate capacitance and related instability effects," *IEEE Electron Device Lett.*, vol. 18, no. 12, pp. 622–624, 1997.
- [39] A. K. Jonscher, "The physical origin of negative capacitance," *J. Chem. Soc., Faraday Trans. II*, vol. 82, pp. 75–81, 1986.
- [40] A. K. Jonscher, *Universal Relaxation Law*, Chelsea Dielectrics Press, London, 1996.
- [41] K. S. A. Butcher, T. L. Tansley, and D. Alexiev, "An instrumental solution to the phenomenon of negative capacitances in semiconductors," *Solid-State Electron.*, vol. 39, no. 3, pp. 333–336, 1996.
- [42] X. L. Huang, Y. G. Shin, K. Y. Lim, E.-K. Suh, H. J. Lee, and S. C. Shen, "Thermally induced capacitance and electric field domains in GaAs/Al_{0.3}Ga_{0.7}As quantum well infrared photodetectors," *Solid-State Electron.*, vol. 41, no. 6, pp. 845–850, 1997.
- [43] N. A. Penin, "Negative capacitance in semiconductor structures," *Semiconductors*, vol. 30, no. 4, pp. 340–343, 1996.
- [44] S. E. Laux, "Techniques for small-signal analysis of semiconductor devices," *IEEE Trans. Comput.-Aided Design Integrated Circuits*, vol. 4, no. 4, pp. 472–481, 1985.
- [45] J. C. McGroddy and P. Guéret, "Dynamic bulk negative differential conductivity in semiconductors," *Solid-State Electron.*, vol. 14, pp. 1219–1224, 1971.
- [46] W. Shockley, "Negative resistance arising from transit time in semiconductor devices," *The Bell System Technical Journal*, vol. 33, no. 4, pp. 799–826, 1954.
- [47] B. F. Levine, "Quantum-well infrared photodetectors," *J. Appl. Phys.*, vol. 74, no. 8, pp. R1–R81, 1993.
- [48] M. Ershov, C. Hamaguchi, and V. Ryzhii, "Device physics and modeling of multiple quantum well infrared photodetectors," *Jpn. J. Appl. Phys.*, vol. 35, Part 1, no. 2B, pp. 1395–1400, 1996.
- [49] A. G. Steele, H. C. Liu, M. Buchanan, and Z. R. Wasilewski, "Influence of the number of wells on the performance of multiple quantum well intersubband infrared detectors," *J. Appl. Phys.*, vol. 72, no. 3, pp. 1062–1064, 1992.

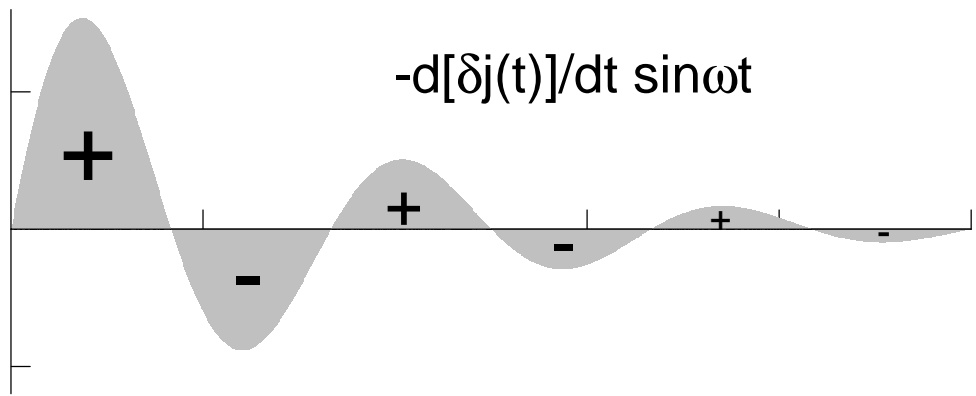
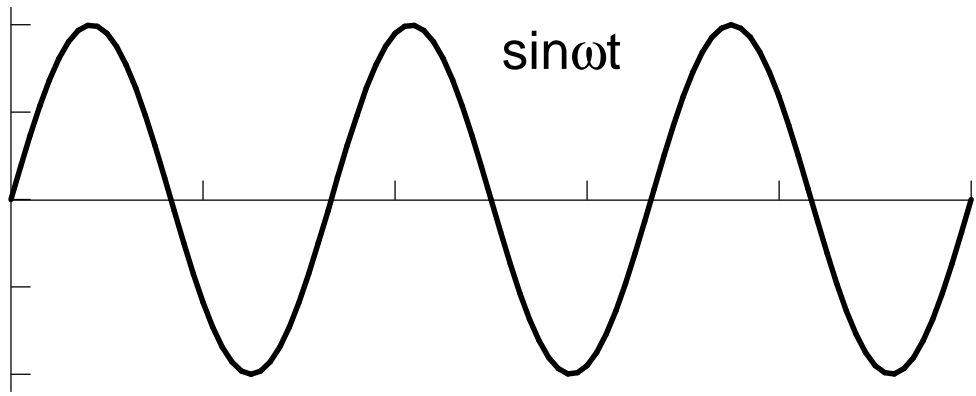
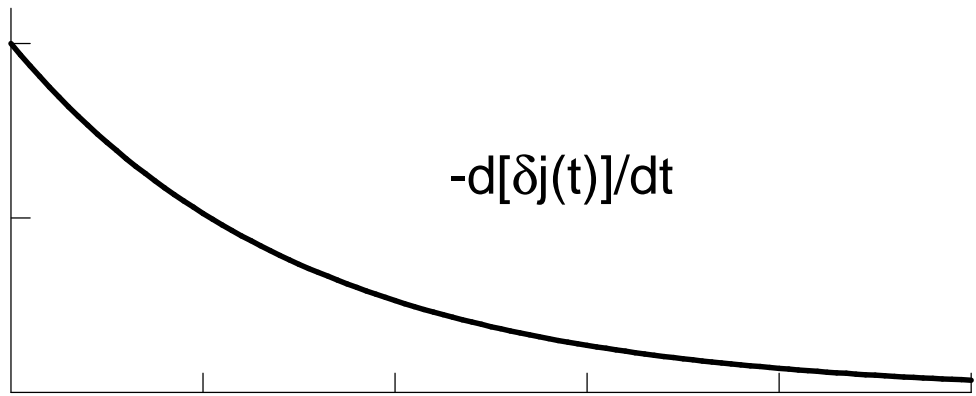
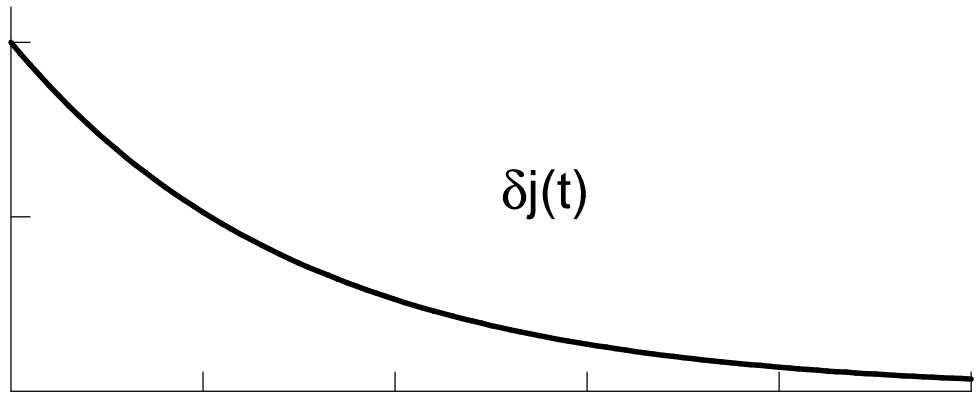
- [50] M. Ershov, V. Ryzhii, and C. Hamaguchi, "Contact and distributed effects in quantum well infrared photodetectors," *Appl. Phys. Lett.*, vol. 67, no. 21, pp. 3147–3149, 1995.
- [51] M. Ershov and V. Ryzhii, "Modeling of multiple InGaAs/GaAs quantum well infrared photodetectors," in *Proceedings of the 7th International Conference on Narrow Gap Semiconductors*, J. L. Reno, Ed. Santa-Fe, NM, January 8–12, 1995, pp. 353–358, IOP, Bristol, 1995.
- [52] V. Ryzhii and M. Ershov, "Electron density modulation effect in a quantum-well infrared phototransistor," *J. Appl. Phys.*, vol. 78, no. 2, pp. 1214–1218, 1995.
- [53] M. Ershov, V. Ryzhii, and K. Saito, "Small-signal performance of a quantum well diode," *IEEE Trans. Electron Devices*, vol. 43, no. 3, pp. 467–472, 1996.
- [54] J.-C. M'Peko, "Effect of negative capacitances on high-temperature dielectric measurements at relatively low frequency," *Appl. Phys. Lett.*, vol. 71, no. 25, pp. 3730–3732, 1997.
- [55] R. Rifkin and Jr. B. S. Deaver, "Current-phase relation and phase-dependent conductance of superconducting point contacts from RF impedance measurements," *Phys. Rev. B*, vol. 13, no. 9, pp. 3894–3901, 1976.

FIGURE CAPTIONS

- Fig. 1. Schematic diagram of (a) transient voltage and (b) transient current in a device excited by a voltage step. The transient current is decomposed into the components corresponding to (c) DC conductivity, (d) displacement current, and (e) relaxation current.
- Fig. 2. Schematic diagram of (a) transient voltage and (b) transient current in a device excited by a voltage impulse. The transient current is decomposed into the components corresponding to (c) DC conductivity, (d) displacement current, and (e) relaxation current.
- Fig. 3. Illustration of the relation between the transient relaxation current and capacitance (eq. (11)) for the case of monotonically decreasing function $[-\delta j(t)/dt]$ ($C(\omega) - C_0 > 0$).
- Fig. 4. (a) Transient relaxation current and (b) capacitance for the analytical model (equations (21)–(22)). The values of the parameters are listed in the inset.
- Fig. 5. (a) Schematic diagram of structure and (b) conduction band profile for a QWIP.
- Fig. 6. Capacitance-voltage characteristics measured at different frequencies. The arrow indicates the value of the geometric capacitance C_0 .
- Fig. 7. Frequency dependence of capacitance on (a) a linear scale and (b) a logarithmic scale for different applied voltages. In (b), absolute value of capacitance is plotted, and the parts of the curves corresponding to negative capacitance values are indicated by arrows.
- Fig. 8. Calculated capacitance-voltage (a) and capacitance-frequency (b) characteristics. In (b), absolute value of capacitance is plotted, and parts of the curves corresponding to negative capacitance values are indicated by arrows.
- Fig. 9. Calculated transient current in response to a voltage step of $\Delta V = 5 \times 10^{-3}$ V at (a) low and (b) high voltages.
- Fig. 10. Emitter electric field E_e and its derivative versus average electric field $E_a = V/L$.
- Fig. 11. Time dependence of (a) the electric field in the emitter barrier and (b) transient current in QWIP in response to a voltage step.







Time (a.u.)

